

Ocean Modelling

journal homepage: www.elsevier.com/locate/ocemod

Dynamic and thermodynamic coupling between the atmosphere and ocean near the Kuroshio current and extension system

Ajin Cho ^a, Hajoon Song ^{a,b}*^a, Hyodae Seo ^c, Rui Sun ^d, Matthew R. Mazloff ^d, Aneesh C. Subramanian ^e, Bruce D. Cornuelle ^d, Arthur J. Miller ^d

^a Department of Atmospheric Sciences, Yonsei University, Seoul, Republic of Korea

^b Division of Environmental Science & Engineering, Pohang University of Science and Technology, Pohang, Republic of Korea

^c Department of Oceanography, University of Hawai'i at Mānoa, Honolulu, HI, USA

^d Scripps Institution of Oceanography, University of California, San Diego, La Jolla, CA, USA

^e Department of Atmospheric and Oceanic Sciences, University of Colorado, Boulder, Boulder, CO, USA

ARTICLE INFO

Dataset link: https://github.com/iurnus/scraps_kaust_model/releases/tag/v1.2, <https://doi.org/10.5281/zenodo.11480617>

Keywords:

Ocean surface currents
Air-sea fluxes
Current feedback
Kuroshio current

ABSTRACT

Relative wind (RW; wind relative to surface currents) has been shown to play a crucial role in air-sea interactions, influencing both atmospheric and oceanic dynamics. While the RW effects through momentum flux are well-documented, those through turbulent heat fluxes remain unknown. In this study, we investigate two distinct surface current feedbacks – those associated with the momentum flux and turbulent heat fluxes – by modifying respective bulk formulations in the regional ocean-atmosphere coupled system, and analyze both immediate and seasonal changes in the boundary layers. Our results show that strong ocean currents in the Kuroshio Current and Extension significantly impact surface coupling, with responses generally contingent on the wind-current angle: an increase (decrease) in air-sea momentum and turbulent heat fluxes occurs when the low-level wind and surface currents are aligned (opposed). The instantaneous responses to surface currents include changes in low-level wind, surface current speed, and humidity, which are consistent with anticipated changes for a given wind-current angle based on the bulk formulations. While the wind-current angle is still an important factor, it does not adequately capture the seasonal responses. On the seasonal timescale, both surface current feedbacks can alter the path of the Kuroshio Extension and mesoscale activities, resulting in different background states that affect air-sea momentum and turbulent heat exchanges. Our results suggest that the energetic current system, such as the Kuroshio Current and Extension, can be significantly influenced by surface current coupling through both momentum and turbulent heat fluxes.

1. Introduction

Air-sea interaction near western boundary currents is characterized by mesoscale oceanic features, such as eddies and sea surface temperature (SST) fronts (Foussard et al., 2019; Kilpatrick et al., 2014; Ma et al., 2015, 2016; Minobe et al., 2008; Putrasahan et al., 2013; Renault et al., 2023; Seo et al., 2008, 2016, 2023; Small et al., 2008). These oceanic features with strong SST gradients leave footprints in the atmosphere by influencing air-sea fluxes (Cronin et al., 2019; Renault et al., 2023). As indicated by Frenger et al. (2013), SST anomalies related to the oceanic eddies modify the turbulence in the atmospheric boundary layer, affecting near-surface wind, cloud properties, and rainfall. These frontal-scale air-sea interactions have mainly been discussed in the context of the atmospheric responses to SST.

In addition to the thermal feedback, which represents the atmospheric response to SST, there is another process through which

mesoscale oceanic phenomena act as pathways for air-sea interactions: the current feedback (CFB) (Renault et al., 2019). As the surface current drives the movement of the interface between the atmosphere and ocean, the low-level wind relative to the surface current influences the transfer of momentum from the atmosphere to the ocean, affecting the atmospheric boundary layer and upper ocean (Chelton et al., 2004; Renault et al., 2017). Due to the CFB, the ocean's eddy kinetic energy (EKE) decreases and the oceanic circulation slows down when the surface current is considered in the momentum flux (Jullien et al., 2020; Renault et al., 2016; Shan et al., 2020; Seo et al., 2016, 2019; Song et al., 2020).

While the CFB through momentum flux is well-documented, little is known about the CFB through air-sea heat and moisture fluxes. The air-sea heat exchange through turbulent heat flux plays a significant

* Corresponding author at: Department of Atmospheric Sciences, Yonsei University, Seoul, Republic of Korea.
E-mail address: hajsong@yonsei.ac.kr (H. Song).

role in the mid-latitude storm track and moisture flux (Cronin et al., 2019). In regions where heat is actively released, such as the Kuroshio current, heat and moisture exchanges at the sea surface are crucial components of the climate system, influencing the intensity of the synoptic weather patterns (Parfitt et al., 2016; Parfitt and Seo, 2018) and shaping the long-term mean and variability of the extratropical atmospheric circulation (Ma et al., 2015; O'Reilly and Czaja, 2015). The air-sea heat and moisture exchanges at the sea surface are proportional to the wind speed relative to the surface current (Cronin et al., 2019).

In this study, we conducted a series of modeling experiments to investigate two different CFBs, namely, the CFBs through the momentum flux (CFB_{τ}) and turbulent heat flux (CFB_Q). To isolate the effects of surface currents on the two air-sea fluxes, we modified the bulk formulation for the air-sea fluxes to include or exclude the impact of surface currents. Furthermore, a statistical approach was employed to ascertain the evolution of the factors determining the response of air-sea fluxes to surface current coupling over time.

In the following section, the methodology employed in this study is presented, including an overview of the coupled ocean-atmosphere model, experimental design, and evaluation to ensure the model's representability. Subsequently, in Section 3, we present the investigation of the spontaneous responses in air-sea fluxes caused by the presence of surface currents. In Section 4, we focus on the seasonal scale responses and investigate how the atmosphere and ocean near the sea surface respond to the CFB. Finally, in Section 5, we discuss the implications of our findings and provide a conclusive summary.

2. Method

2.1. Coupled ocean-atmosphere model

In this study, we investigated the effect of current coupling using the regional coupled ocean-atmosphere model, namely, Scripps-KAUST Regional Integrated Prediction System (SKRIPS) v1.2 (Sun et al., 2019). In this model, the ocean model, MIT general circulation model (MITgcm, Marshall et al. (1997)), and atmospheric model, Weather Research and Forecasting (WRF, Skamarock et al. (2019)), are combined through the Earth System Modeling Framework (ESMF) coupler (Hill et al., 2004). WRF transmits the following data to the MITgcm: 2-m specific humidity, 2-m air temperature, 10-m wind, moisture flux, precipitation, surface pressure, and surface heat fluxes. In return, MITgcm transmits the SST and surface current data to WRF. The model domain covers the area from the equator to 52°N and from 117°E to 157°E, representing the western North Pacific region. The horizontal resolution of both models is 0.1°; thus, the grid size is approximately 11 km around the Kuroshio Extension, which is suitable for simulating mesoscale ocean eddies. The oceanic initial and boundary fields for MITgcm are obtained from the Ocean Reanalysis System 5 (ORAS5) (Zuo et al., 2019). In MITgcm, 90 vertical levels are used, with a minimum spacing of 1 m near the sea surface that gradually increases to over 100 m for the bottom layers. WRF utilizes a non-hydrostatic configuration with 40-eta levels in the vertical direction and an upper level at 50 hPa. The atmospheric initial and boundary fields are obtained from the European Centre for Medium-Range Weather Forecasts Reanalysis v5 (ERA5) (Hersbach et al., 2020). The time steps for both models and coupling interval are 30 s.

WRF employs a variety of physical schemes, including the Rapid Radiative Transfer Model for GCMs (RRTMG) longwave and shortwave (Iacono et al., 2008), WSM6 microphysics (Hong and Lim, 2006), Mellor-Yamada-Nakanishi-Niino (MYNN) surface layer and planetary boundary layer (Nakanishi and Niino, 2004, 2009), unified Noah land surface, and new Tiedtke cumulative schemes. The MYNN surface layer scheme was modified to include or exclude the surface current to estimate momentum and heat fluxes, as discussed in Section 2.2.

Table 1

Description of the simulation experiments. ρ_a represents the air density, C_D is the drag coefficient, \mathbf{W} is the wind vector, and \mathbf{U} is the surface current vector. L_e denotes the latent heat of vaporization, C_E is the latent heat transfer coefficient, c_p represents the specific heat capacity at constant pressure, and C_H is the sensible heat transfer coefficient. LHF and SHF are the latent and sensible heat fluxes, respectively.

Case name	RW	τ_{AW}	Q_{AW}
Wind stress	$\rho_a C_D \mathbf{W} - \mathbf{U} (\mathbf{W} - \mathbf{U})$	$\rho_a C_D \mathbf{W} (\mathbf{W})$	$\rho_a C_D \mathbf{W} - \mathbf{U} (\mathbf{W} - \mathbf{U})$
LHF	$\rho_a L_e C_E \mathbf{W} - \mathbf{U} \Delta q$	$\rho_a L_e C_E \mathbf{W} - \mathbf{U} \Delta q$	$\rho_a L_e C_E \mathbf{W} \Delta q$
SHF	$\rho_a c_p C_H \mathbf{W} - \mathbf{U} \Delta T$	$\rho_a c_p C_H \mathbf{W} - \mathbf{U} \Delta T$	$\rho_a c_p C_H \mathbf{W} \Delta T$

2.2. Experiments

Although there have been studies aimed at improving the parameterization of air-sea fluxes in ocean-atmosphere coupled systems (Pelletier et al., 2021), for simplicity, the COARE 3.0 bulk formulae (Fairall et al., 2003) calculates the wind stress and turbulent heat flux using 10-m wind relative to the surface current. In the ocean model, momentum flux is calculated based on the 10-m wind. To exclude the effect of surface currents from wind stress and heat flux calculations, we used the absolute wind as a 10-m wind input to the bulk formula. Subsequently, by modifying the bulk formation of turbulent heat fluxes to use the absolute wind in the friction velocity, the effect of surface currents on the turbulent heat flux can be eliminated. To investigate the changes in wind stress (τ) and upward turbulent heat flux (Q ; a sum of upward latent and sensible heat fluxes) triggered by the surface currents and subsequent feedback, we conducted three experiments (Table 1). In the names of the simulation cases, RW (AW) refers to the relative (absolute) wind. RW is the control simulation, wherein the effect of surface currents on both the momentum and turbulent heat fluxes are considered as set by default. τ_{AW} excludes the effect of surface currents from the momentum flux calculation, whereas Q_{AW} excludes this effect from turbulent heat flux calculations. The freshwater flux associated with evaporation in RW is also affected by the surface currents. By comparing RW with τ_{AW} , the CFB through the momentum flux (CFB_{τ}) can be identified, whereas comparing RW with Q_{AW} reveals the CFB through the turbulent heat flux (CFB_Q).

The changes in air-sea fluxes due to the relative wind effect on heat and momentum fluxes could affect the lower atmosphere and upper ocean. The initial changes can be anticipated by the bulk formulation, but subsequent feedback between the lower atmosphere and upper ocean layer can lead to divergences in the mean states of the atmosphere and ocean. Once the feedback processes are triggered, the attribution of the differences between simulations to the current effects or altered atmospheric and oceanic conditions becomes complex. Hence, we explored two different timescales. The first timescale is 5 min after the start of the simulations, capturing the immediate responses before large-scale feedback have begun. Although the first PBL time step (30 s) could have been chosen, it might not be long enough for the signals to develop sufficiently to be captured. The second timescale spans six months to contain complicated feedback between the atmosphere and ocean in the seasonal timescale.

We used the results from two sets of six-month integrations, starting from January 1 and June 30, 2016, respectively. The first set includes the RW, τ_{AW} , and Q_{AW} cases initialized on January 1, and these results are presented in the main text. To assess seasonal dependence, we also analyzed RW, τ_{AW} , and Q_{AW} cases that diverged from the RW state on June 30, with their results shown in the supplementary information. The results from January 1 to June 29 are not spin-up, while the simulations from June 30 to December 31 diverged from a fully spun-up RW state. A comparison of the main text and supplementary information demonstrates that both seasonal dependence and spin-up dependence are minimal.

2.3. The evaluation of the air-sea fluxes

To compare the air-sea flux of the model with observations, we used the third-generation Japanese Ocean Flux datasets using Remote

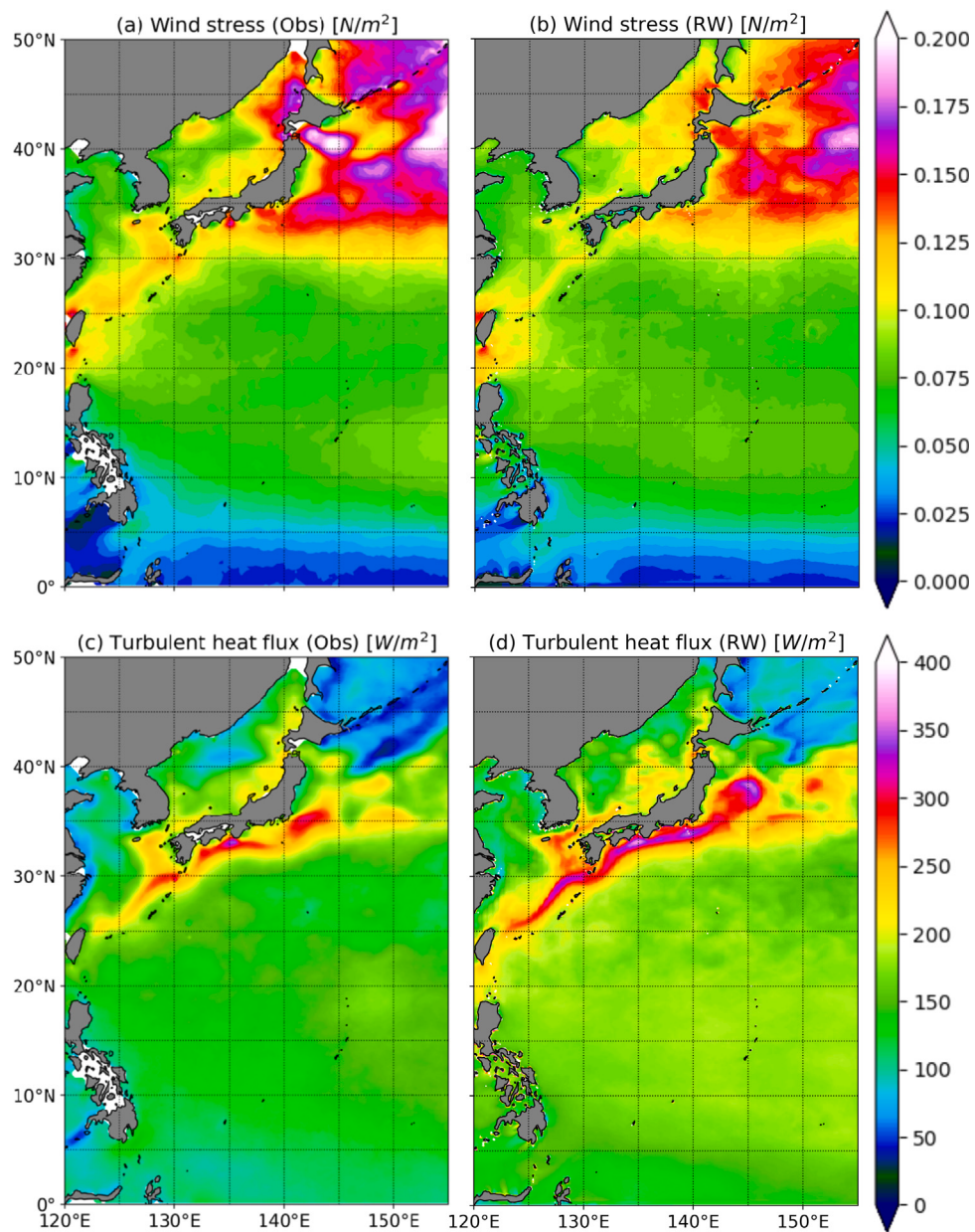


Fig. 1. Annual mean maps of (a,b) wind stress and (c,d) turbulent heat flux from the (a,c) J-OFURO3 data and (b,d) RW simulation.

sensing Observations (J-OFURO3) (Tomita et al., 2019). J-OFURO3 contains the datasets for surface heat, momentum, and freshwater fluxes with daily and monthly means, with a spatial resolution of 0.25° over the global oceans from 1988 to 2017.

The annual mean wind stress and turbulent heat flux from the RW simulation are evaluated against the J-OFURO3 data (Fig. 1). The spatial pattern of the wind stress in the RW simulation was in good agreement with that of J-OFURO3, with a spatial correlation coefficient of 0.96 (Fig. 1(a,b)). The turbulent heat flux of the model was slightly overestimated when compared with that of J-OFURO3, particularly near the Kuroshio current and Kuroshio Extension (Fig. 1(c,d)). This discrepancy can be attributed to the warm SST bias in the model, resulting in greater heat loss. However, the bias in the turbulent heat flux is not expected to alter the conclusions of our study when discussing the impact of the surface current on the air-sea fluxes. Furthermore, the spatial correlation coefficient was 0.86, suggesting that the model satisfactorily simulated the air-sea turbulent heat flux.

3. Immediate responses

The initial responses of the atmospheric and oceanic states near the air-sea interface were examined in the first 5-min integration. This was conducted to investigate the effect of ocean currents on air-sea fluxes before the onset of the feedback effects. The spontaneous changes in the air-sea fluxes owing to the effect of ocean currents depend on the vector difference of the wind and ocean currents (Fig. 2(g)). Stronger currents are likely to lead to more significant air-sea flux modulation, and the sign of these alterations depends on the angle between the low-level wind and current vectors (wind-current angle). Specifically, the wind-current angle is 0° when the low-level wind and surface currents are perfectly aligned, 90° when they are perpendicular, and 180° when they are opposed.

The immediate responses to the changes in air-sea fluxes can be anticipated for some variables that are directly influenced by these fluxes (Fig. 2(a-f)). For example, the modification in the momentum

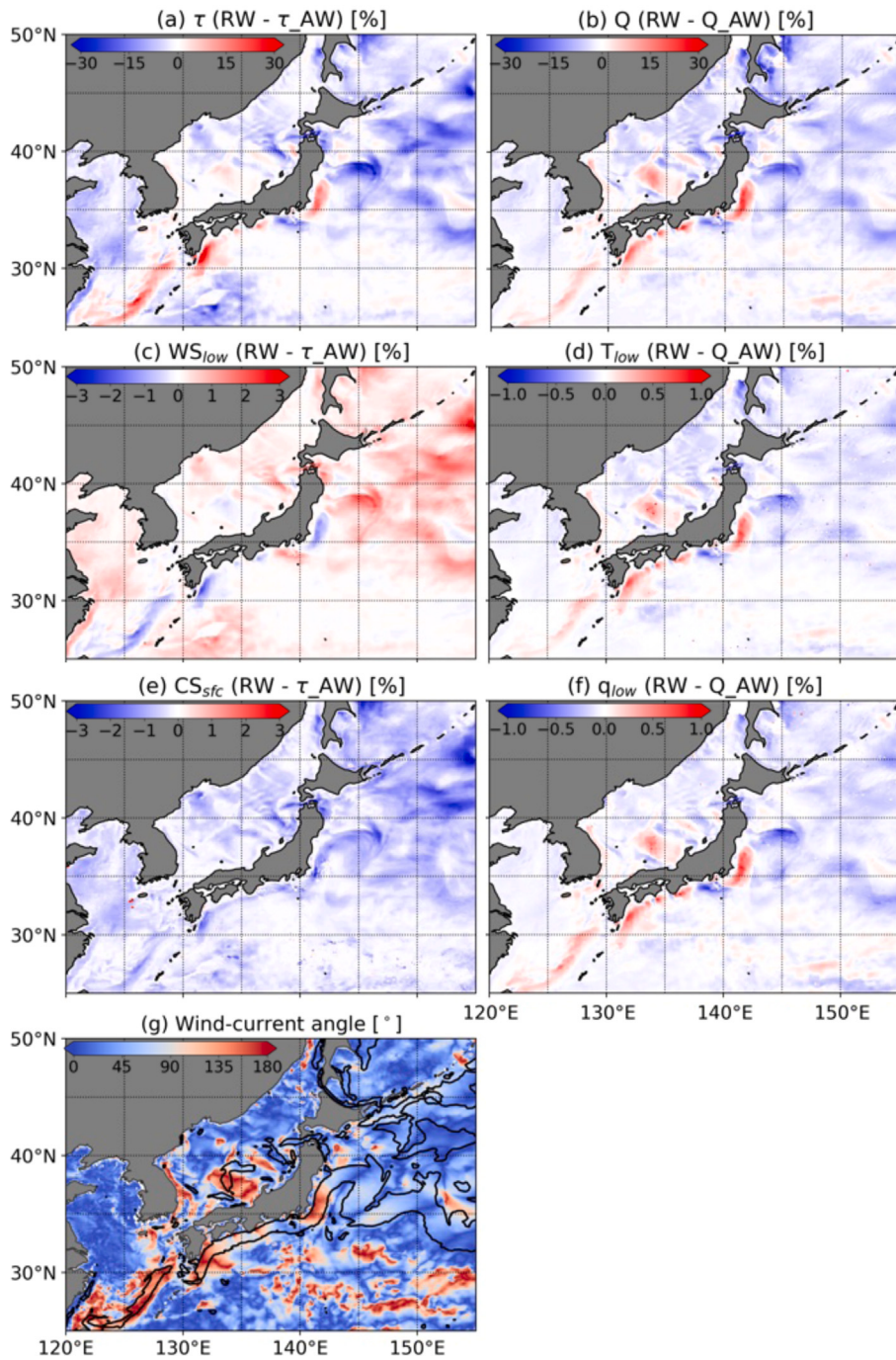


Fig. 2. The differences within the first 5-min integration between RW and either τ_{AW} or Q_{AW} . The differences between RW and τ_{AW} in the (a) wind stress magnitude, (c) lowest level wind speed, and (e) surface current speed are shown as the percentage changes relative to their daily standard deviations. Similarly, the percentage differences between the RW and Q_{AW} are examined for the (b) turbulent heat flux, (d) lowest level temperature, and (f) water vapor mixing ratio. The shading in (g) represents the angle between the lower-level wind and surface current vectors, and the contours indicate the location where the surface current speeds exceed 0.3 m/s.

flux will likely impact the lower atmospheric wind and surface currents owing to changes in momentum exchange or drag. Modulations in the turbulent heat fluxes are expected to influence the lower atmospheric temperature and humidity. The differences in these variables between the simulations were first evaluated after normalizing them by the standard deviation determined from the six-month simulation.

Modulations in air-sea fluxes are particularly pronounced in regions with stronger currents (≥ 0.3 m/s), wherein the sign of the differences varies with the angle. The differences in wind stress and turbulent heat flux between the RW and AW cases exhibit similar patterns (Fig. 2(a,b)), with generally smaller air-sea fluxes being observed in

RW simulations. This is because the current tends to align parallel to the surface wind in most areas (Fig. 2(g)); thus, the magnitude of the relative wind is smaller than that of the absolute wind. However, in locations where the current opposes the wind, the wind stress and turbulent heat fluxes are larger in the RW simulation. Notably, differences are more significant in the wind stress owing to the quadratic influence of currents in the bulk formulation of wind stress.

The alterations in air-sea fluxes also result in immediate responses in the lower-level atmosphere and sea surface. The difference in lower-level wind speed has the opposite sign to those in wind stress (Fig. 2(c)), indicating that the region with diminished wind stress experiences

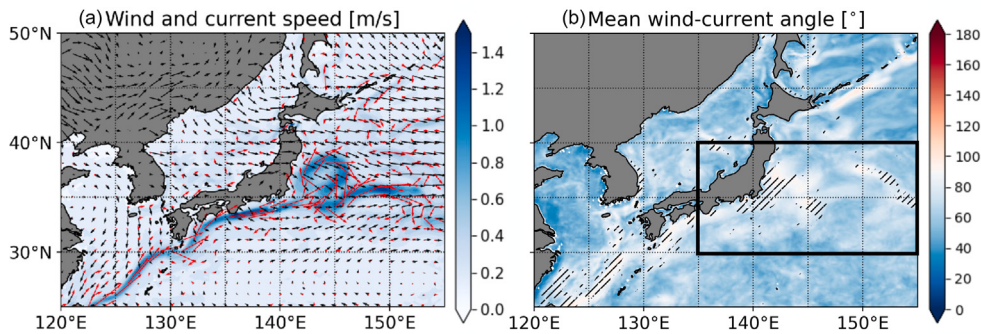


Fig. 3. (a) The 6-month averaged surface current speeds (shading), lower-level wind (black arrows), and surface current (red arrows) in the RW simulation. (b) The 6-month averaged wind-current angle for the RW simulation. The hatched areas represent the regions where the interquartile ranges of the wind-current angle are larger than 90°. The black square in (b) represents the area for the Kuroshio Extension used in the analysis.

faster lower-level winds identified here as the wind at the lowest atmospheric model level. This phenomenon can be attributed to the fact that the atmosphere generally loses a smaller amount of momentum to the ocean in the RW simulation than τ_{AW} . The differences in the lower-level temperature and water vapor mixing ratio tend to have the same sign as those in the turbulent heat flux as the heat and moisture source for the lower atmosphere (Fig. 2(d, f)). The differences in the surface current speed exhibit negative values across the majority of the region (Fig. 2(e)). This effect can be explained by examining the wind work, which represents the work done by the wind on the ocean surface. The expressions for wind work in RW and τ_{AW} are given below:

$$w_{RW} = \rho C_D |\mathbf{W} - \mathbf{U}| (\mathbf{W} \cdot \mathbf{U} - \mathbf{U} \cdot \mathbf{U})$$

that for τ_{AW} is:

$$w_{AW} = \rho C_D |\mathbf{W}| (\mathbf{W} \cdot \mathbf{U})$$

ρ_a represents the air density, C_D is the drag coefficient, \mathbf{W} is the wind vector, and \mathbf{U} is the surface current vector. In areas where the low-level wind and surface current are aligned, the wind work is positive but less so in RW than in τ_{AW} . In contrast, where the low-level wind and surface currents are oppose each other, the wind work is negative and is more strongly negative in RW compared to τ_{AW} . This leads to a general slowing down of the surface currents in RW relative to τ_{AW} in both areas.

These findings reveal that the current effects not only induce immediate changes in air-sea fluxes but also in both the lower atmosphere and upper ocean. The spontaneous responses are in general agreement with the changes anticipated from the bulk formulation. These responses are influenced by the magnitude of surface currents and the angle between the wind and current vectors, showing similar spatial patterns (Fig. 2(g)). The exception, in this case, is the surface current, which slows down either by reduced momentum transfer when the current is in a similar direction to the low-level wind or by enhanced drag when it flows in the opposite direction to the wind. The continuous air-sea interactions trigger the feedback mechanisms initiated by the immediate responses, leading to changes in the atmospheric and oceanic states at a seasonal scale, which can complicate the quantification of the direct impacts from the modification of surface current coupling.

4. The responses in seasonal timescale

The changes in momentum, heat, and moisture exchange at the sea surface owing to surface current coupling are expected to result in variations in the atmospheric boundary layer and upper ocean, which, in turn, influence the surface current coupling effect at the

seasonal timescale. For example, in regions where the consideration of surface current coupling reduces the transfer of momentum from the atmosphere to the ocean, a reduction in surface current speed and an increase in lower atmospheric wind speed can be expected. This increase in wind speed would increase the wind stress, thereby increasing momentum transfer in the end. This implies that the initial deceleration of the surface current by wind-current coupling may eventually be partially recovered on a longer timescale by the faster lower-level wind and, in turn, the increased momentum transfer. A similar interaction is anticipated for the turbulent heat flux. In areas where the turbulent heat loss in τ_{AW} surpasses that in RW, the consideration of the current would reduce the heat transfer from the ocean to the atmosphere. This would result in an increase in the SST and a decrease in the lower atmospheric temperature and humidity, resulting in an increase in the differences of temperature and humidity between the atmosphere and ocean. Consequently, the sensible and latent heat fluxes from the sea surface to the atmosphere would increase, indicating negative feedback. In this section, we examined whether these changes over time lead to a diminishing effect of surface current coupling, and explored the seasonal response of the atmosphere and ocean to current coupling.

In the previous section, we emphasized the importance of the current speed and wind-current angle in determining the impact of surface current coupling (Fig. 2). At the seasonal scale, particularly in the mid-latitudes, the direction of the surface wind fluctuates, thereby leading to the time-dependent wind-current angle. Fig. 3 shows the wind and current vectors averaged over six months. In most areas, the averaged wind-current angle is approximately 60°. However, in regions with relatively fast current speeds, the wind-current angles tend to be larger than 60°. The wind-current angle in these regions also shows relatively large variability, as evidenced by the difference between the first and third quartiles of the wind-current angle distribution, which exceeds 90° (the hatched regions in Fig. 3(b)). The significant fluctuations in the wind-current angle at the seasonal scale indicate that the mean angle may not be an optimal metric for discerning the influence of the wind-current angle on the air-sea interactions. Thus, we investigated the responses to surface current coupling by categorizing the daily wind-current angle with a focus on the Kuroshio Extension region (black box in Fig. 3(b)). This region was selected owing to its substantial momentum and turbulent heat exchange, as shown in Fig. 1, but also large temporal variability in the wind-current range Fig. 3(b).

4.1. Changes in the air-sea fluxes and states near the interface by current coupling

The current coupling alters the air-sea exchanges, as well as the states of the lower atmosphere and upper ocean, which still tends to depend on the wind-current angle. The histogram of the differences in

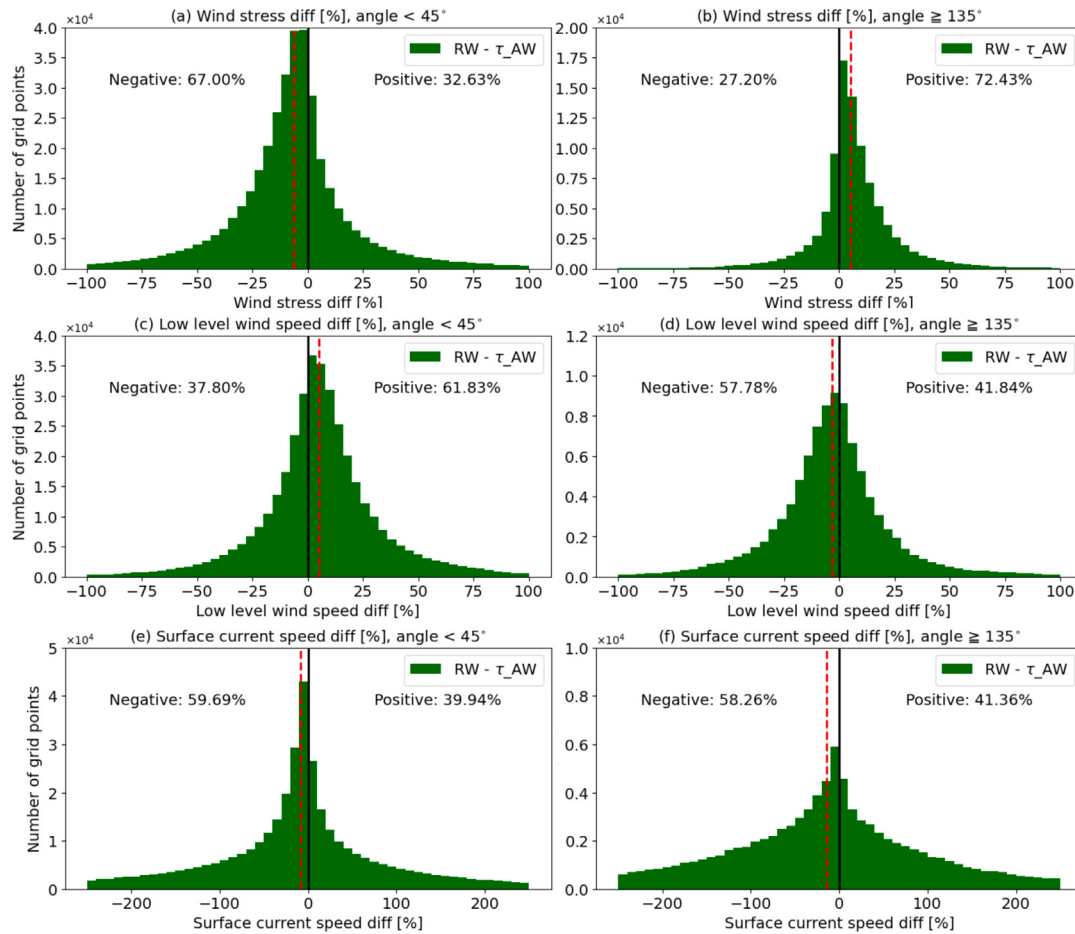


Fig. 4. The histogram of the daily mean difference [%] between RW and τ_{AW} in (a,b) wind stress, (c,d) low-level wind speed, and (e,f) surface current speed for grid points with surface currents larger than 0.3 m/s in the Kuroshio Extension (black box in Fig. 3(b)). Panels (a,c,e) are the cases when the daily wind-current angle is below 45°, and (b,d,f) are those when it is between 135° and 180°. The red dashed lines show the medians of the differences.

wind stress, low-level wind speed, and surface current speed between RW and τ_{AW} indicates that the seasonal-scale changes in these variables are similar to the spontaneous responses (Figs. 2 and 4). When the wind and current directions are aligned, the wind stress in RW is lower than that in τ_{AW} in more than half of the selected points, whereas it is larger in the other case (Fig. 4(a,b)). The differences in the low-level wind speed demonstrate a shift toward positive (negative) values in areas where the angle is below 45° (above 135°). This is consistent with the anticipated effects of changes in the wind stress. The reduced wind stress leads to faster lower-level winds owing to the reduced momentum loss to the ocean. Conversely, the surface current speed uniformly decreases, similar to the spontaneous response.

We further investigated whether the responses driven by CFB_Q during the spontaneous response were also manifested on a seasonal scale. Fig. 5 shows the differences in the turbulent heat flux, moisture flux, and SST between RW and Q_{AW} . As anticipated from the bulk formulation, the turbulent heat flux and moisture flux are reduced in more than half of the points in RW when the wind-current angle is below 45° over a seasonal timescale (Fig. 5(a,c)). Considering angles above 135°, the differences in turbulent heat flux and moisture flux showed clear shifts to positive signs when surface current coupling was considered (Fig. 5(b,d)). Notably, the differences in SST exhibit minimal shifts of medians in both angle conditions, suggesting that current coupling leads to insignificant changes in SST (Fig. 5(e,f)), possibly owing to other important processes, such as shortwave radiation and the advection. In general, the wind-current angle is an important factor in modifying the air-sea fluxes, and for the boundary layers of the atmosphere and ocean, even on a seasonal timescale.

4.2. Changes in the background states by current coupling

We explore how the surface current modulates the air-sea fluxes as a function of the surface current speed and wind-current angle, and how these relationships vary over time. Accordingly, we employ conditional mean plots, which classify all grid points within the analyzed area based on the wind-current angle and surface current speed. The bins are defined with an interval of 0.1 m/s for the surface current speed on the x-axis and an interval of 10° for the wind-current angle on the y-axis. The data used to define these bins were derived from the RW simulation over the Kuroshio Extension (as delineated by the black box in Fig. 3(b)) to explore how these factors alter the air-sea fluxes and surface quantities. If the changes in air-sea fluxes by the effects of the current are solely attributed to surface current speeds, the variation is expected to occur only along the x-axis while remaining constant along the y-axis. Conversely, if the wind-current angle is the only influencing factor, the variation would occur only along the y-axis. If both factors interact, changes would occur in both directions.

The differences in both τ and Q exhibit a pattern of sign changes at approximately 80~100° (Fig. 6(a,c)) in the first month. This pattern is consistent with the that derived from the bulk formulation. The magnitude of the differences generally increases with the surface current speed. When the current speed is below 0.2 m/s, the difference in τ or Q is nearly zero.

The six-month integration alters the conditional mean plots of the differences in τ and Q as the RW and other AW cases diverge (Fig. 6(b,d)). In the case of τ , insignificant differences were observed at lower current speeds (≤ 0.2 m/s), which was similar to those of the case

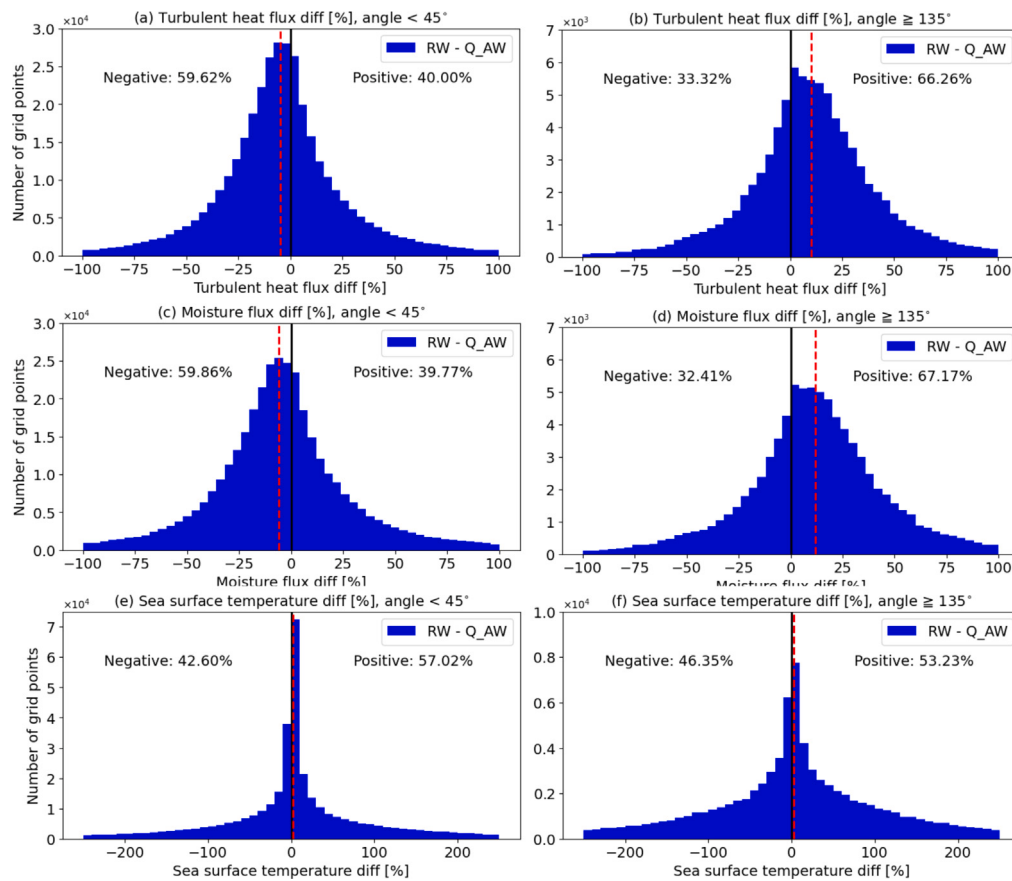


Fig. 5. Same as Fig. 4 but for the differences in (a,b) turbulent heat flux, (c,d) moisture flux, and (e,f) sea surface temperature.

in the first month. The differences in τ stand out at the current speed larger than that, with the sign changes occurring at approximately 45° (Fig. 6(b)). A comparison of the differences in τ in the first month with those in the sixth month reveals that the wind speed in RW is faster than in τ_{AW} , resulting in a reversal of the difference in τ in the bins with an angle between 45° and 90°.

Notably, the wind speed in RW is faster than in τ_{AW} when the angle between the wind and surface current is approximately lower than 120° after six months of integration (Fig. 7(a)). The faster wind speed can be attributed to the decreased momentum loss to the ocean when the angle is smaller than approximately 90° in the RW simulation. Another factor is the higher SST in the RW simulation (Fig. 7(b)). The bins with a current speed greater than approximately 1 m/s are likely located along the Kuroshio Extension, which carries warmer water from the south. Fig. 8(a) shows the averaged sea surface height (SSH) in the fifth and sixth months in RW, where a significant gradient is observed at an SSH of approximately 0.4 m. Assuming the 0.4 m contours as a representation of the Kuroshio Extension or nearby eddies, it is clear that the current coupling alters their positions (Fig. 8(b)). In the RW simulation, the paths of the Kuroshio Extension (black contours in Fig. 8(b, c)) are typically situated northward compared to those in the τ_{AW} simulation (green contours in Fig. 8(b, c)). This suggests that warmer SSTs tend to induce anomalously higher wind speeds, consequently leading to greater wind stress.

The differences in the turbulent heat flux, Q , after six months of integration also differ from those observed in the first month (Fig. 6(c,d)). The Q is lower in RW where the current is weak but greater where the current speed is greater than approximately 1 m/s (Fig. 6(d)). Considering that the differences in Q are largely independent of the wind-current angle and that the turbulent heat flux depends on the SST, the differences in SST between RW and Q_{AW} are more important than the effect of relative wind near the Kuroshio Extension, which is

represented by bins with a current speed of greater than approximately 1 m/s. Fig. 7(c) suggests that the SST is warmer in RW at regions with current speeds faster than approximately 1 m/s, resulting in greater turbulent heat loss in RW. The differences in SST arise from those in the locations of the Kuroshio Extension and eddies between RW and Q_{AW} (black and blue contours in Fig. 8(b, d)). Notably, the consideration of the surface current in the calculation of air-sea fluxes alters the position of the Kuroshio Extension and eddies over a period of six months (Fig. 8(c,d)).

The shift in the Kuroshio Extension and eddies by current coupling is an important factor in interpreting Fig. 6. As the bins in Fig. 6 were created based on the wind-current angle and surface current speed from the RW simulation, the changes in the oceanic conditions owing to CFB at the seasonal scale include the modification of the atmospheric and oceanic conditions near the interface. In particular, the altered Kuroshio Extension and eddies play an important role in this phenomenon. For example, regions with high current speeds in RW are mainly present in the Kuroshio Extension, which transports anomalously warm water from the tropics and is expected to have higher SST. These are not the regions where the Kuroshio Extension passes in Q_{AW} , and their SSTs are lower than those in RW. Hence, the turbulent heat loss in these bins is greater in RW than in Q_{AW} . The discrepancy in the location of the Kuroshio Extension between RW and τ_{AW} also contributes to the differences in SST, resulting in higher SST in RW in the bins whose current speed is greater than 1 m/s (not shown).

The surface current, which is often not considered in the air-sea fluxes, is known to exert impacts on both very short and seasonal timescales. The impacts on the very short timescale are generally consistent with those anticipated by the bulk formulation, indicating changes in the air-sea fluxes and atmospheric and oceanic states near the interface. In the seasonal timescale, the impacts of changes in the

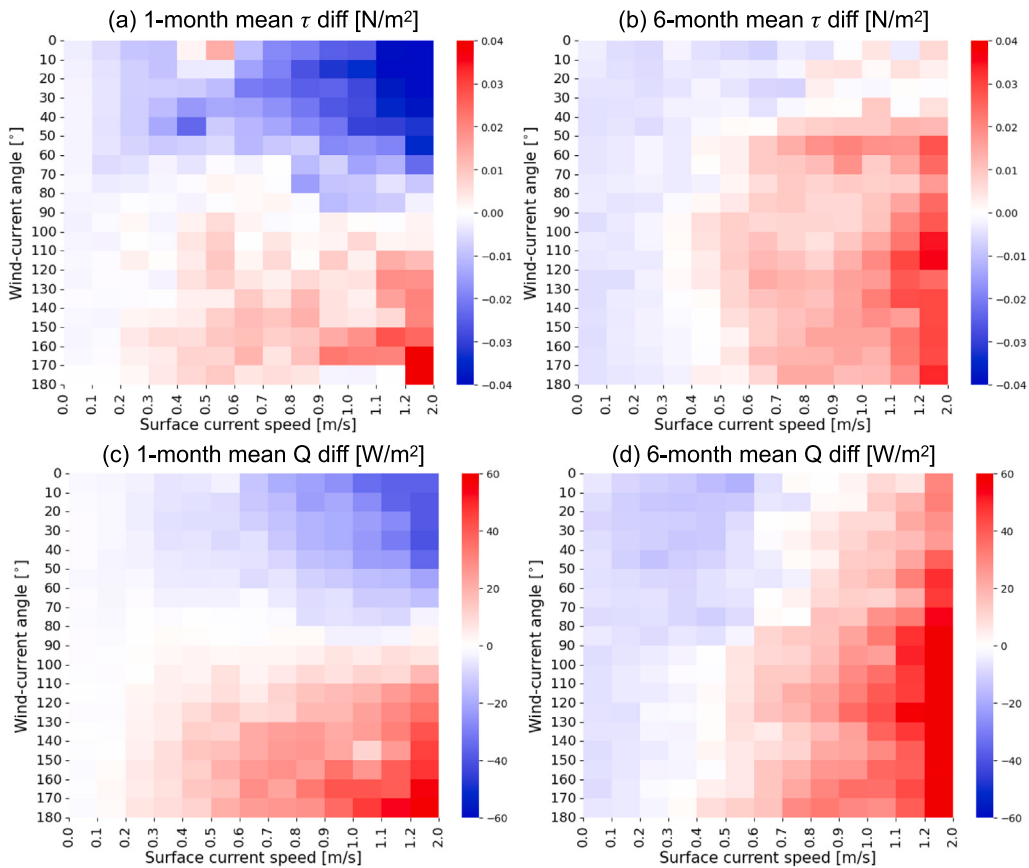


Fig. 6. Conditional mean plots for the (a,b) daily mean difference in wind stress ($RW - \tau_{AW}$) and (c,d) difference in turbulent heat flux ($RW - Q_{AW}$) in the Kuroshio Extension (black box in Fig. 3(b)). (a,c) The differences of the wind stress and turbulent heat flux in the first month; (b,d) the differences in the 6-month averages of the wind stress and turbulent heat flux. Bins are divided into surface current speed and wind-current angle.

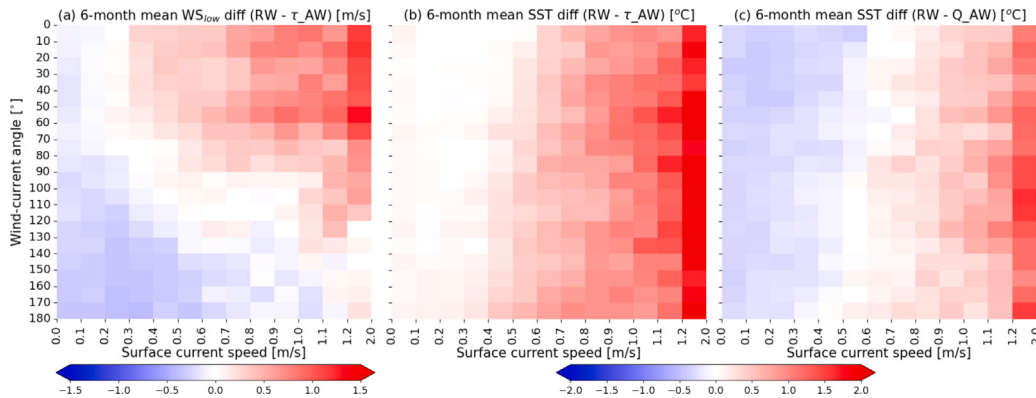


Fig. 7. Conditional mean plots for the (a) lowest level wind speed difference, (b) SST difference between RW and τ_{AW} , and (c) SST difference between RW and Q_{AW} in the sixth month. Bins are divided into surface current speed and wind-current angle of the RW simulation.

mean atmospheric and oceanic states are augmented by the existing short-timescale impacts of the surface current. Despite the negative feedback being expected to dampen the effects of surface current coupling, the average SST and current speed undergo changes, particularly in the region of the Kuroshio Extension. This highlights the importance of surface currents in air-sea interaction.

4.3. Seasonality of the impact of current coupling

The responses to air-sea current coupling vary seasonally due to changes in atmospheric and oceanic conditions, particularly in the Kuroshio Extension region. In winter, winds are generally stronger,

leading to greater wind stress compared to summer. Additionally, cold and dry winter air passing over the ocean creates a large temperature difference between the atmosphere and ocean and highly undersaturated conditions, resulting in greater turbulent heat flux. While the pattern of changes due to current coupling remains consistent across seasons (Figs. 4–5 and S1–2), the magnitude of these changes is more pronounced in winter (Figs. 6(a, c) and 9(a, c)).

This can be identified by the comparison between simulations from January to June, capturing winter and spring responses (Figs. 4–8) and from July to December highlighting summer and autumn responses (Figs. 9–10 and S1–S2). The surface fluxes and near-surface states show a stronger response in winter, with larger shifts of the median from zero

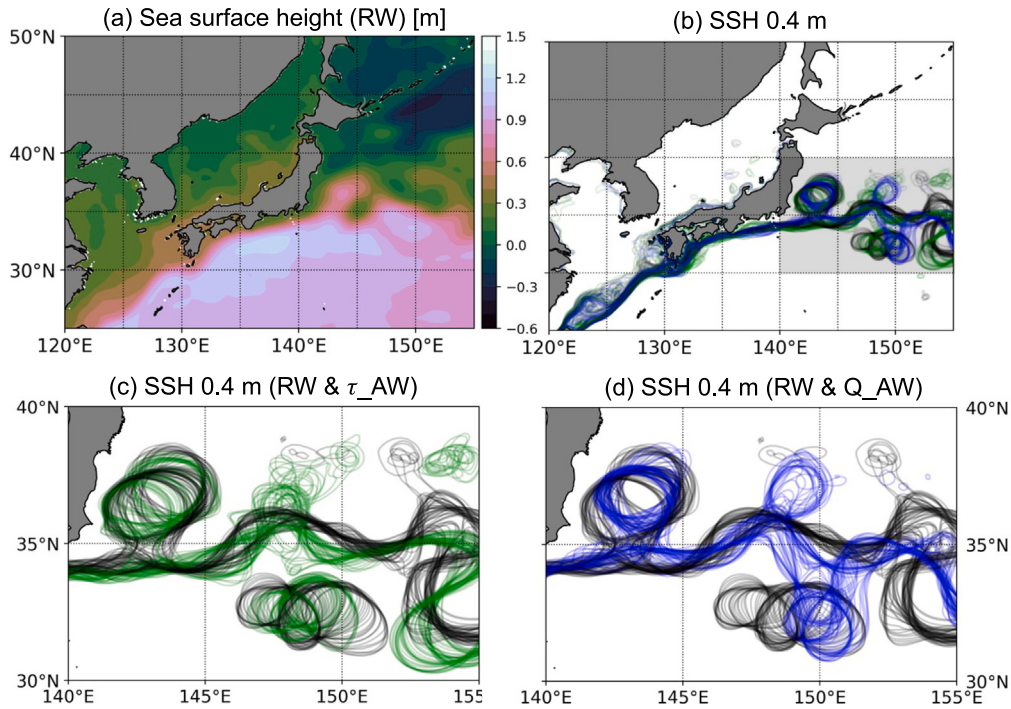


Fig. 8. (a) Mean SSH (m) in RW. (b-d) Daily path of the Kuroshio Extension during the fifth and sixth months of the simulations, represented by the 0.4 m contour of SSH for the RW (black), τ_{AW} (green), and Q_{AW} (blue) simulations.

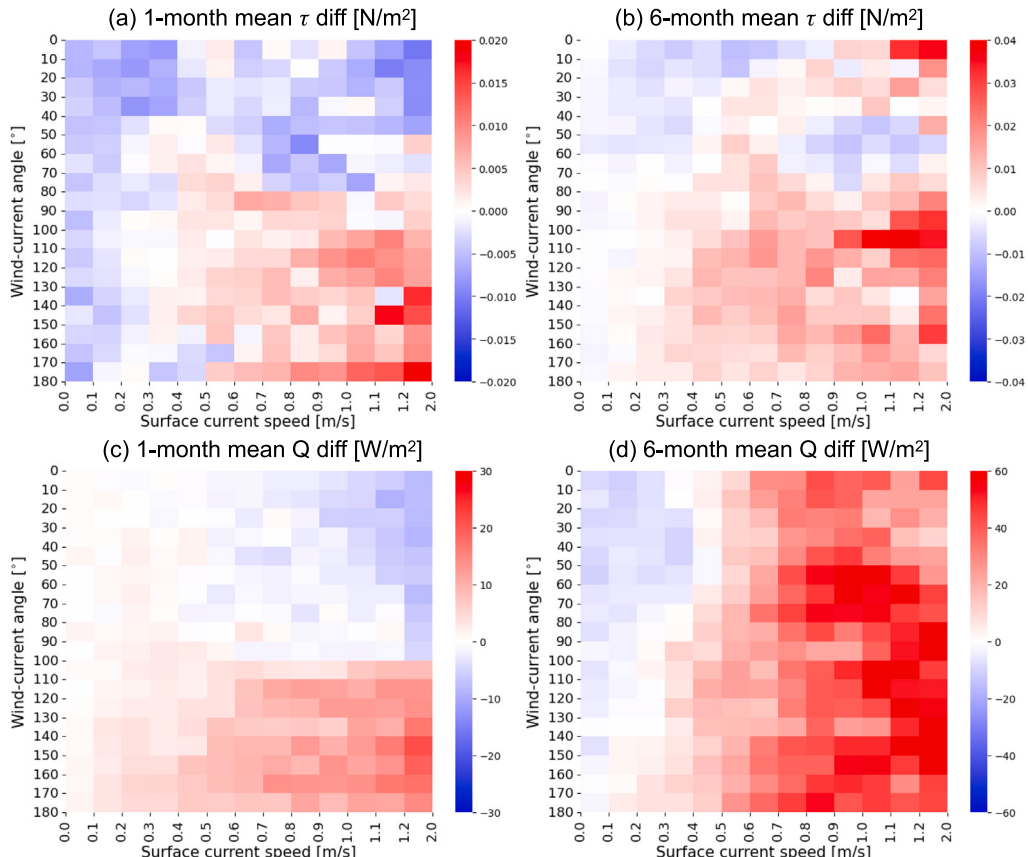


Fig. 9. Same as Fig. 6 but using the simulation output from June 30 to December 31.

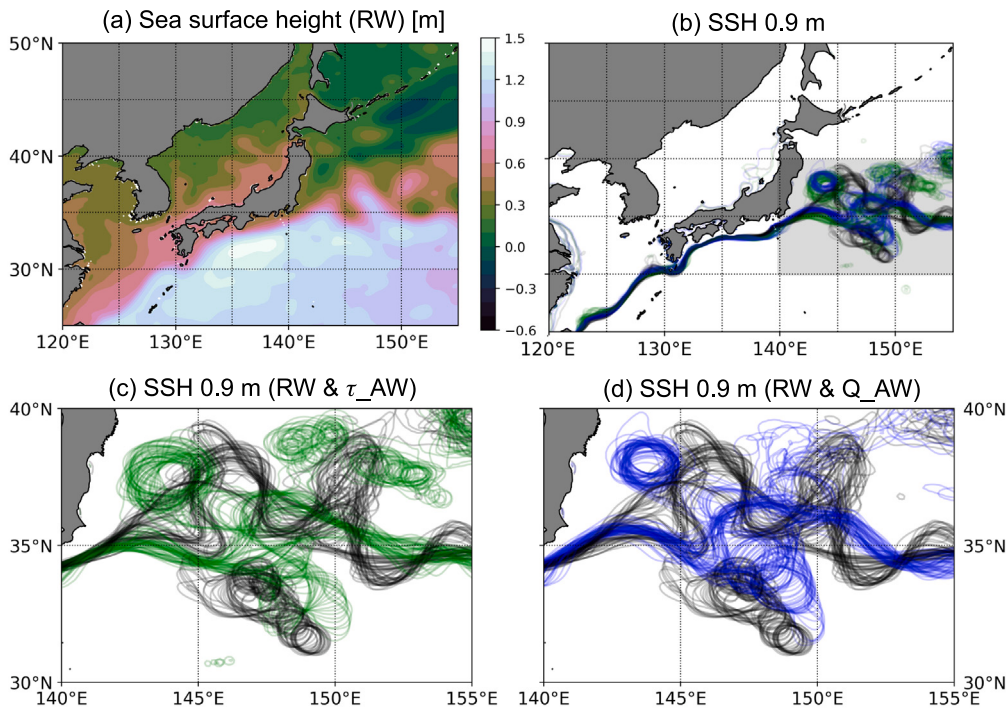


Fig. 10. Same as Fig. 8 but using the simulation output from June 30 to December 31.

in the winter and spring results (Figs. 4,5 and S1,S2). The first-month sensitivities of the wind stress and turbulent heat flux to current speed and wind-current angle do not show significant seasonal differences between winter (Fig. 6.(a,c)) and summer (Fig. 9(a,c)). In both seasons, the differences increase with surface current speed, and the sign of the differences reverses around wind-current angle of 90°, displaying a similar pattern. However, the magnitude of the difference in Fig. 6.(a,c) is approximately twice as large.

The changes in background states after several months of model integration are more pronounced in winter. Although the six-month sensitivities of wind stress are comparable between winter and summer, those for turbulent heat flux are greater in winter (Figs. 6(b,d) and 9(b,d)). The paths of the Kuroshio Extension, represented by the 0.4 m SSH isolines, also show a greater degree of difference between experiments in winter (Figs. 8 and 10). These results suggest that seasonal changes in background states due to current coupling are amplified in winter. In conclusion, while the trends in changes in air-sea fluxes and states near the interface are consistent between summer and winter, their magnitudes are larger in winter. This is also applied to the background state changes by current coupling.

5. Discussion and conclusion

In this study, we investigated the impact of surface currents on air-sea momentum and turbulent heat fluxes in both short and seasonal timescales over the Kuroshio Extension using a fully coupled ocean-atmosphere model. The immediate impacts of current coupling on the states of the atmosphere and ocean near the interface and the fluxes between them are consistent with those determined from the bulk formulation. The current coupling alters the momentum flux depending on the current speed and angle between the wind and current, which, in turn, changes the lower-level wind and current speed. The turbulent heat and moisture fluxes are also modified by current coupling, wherein the current speed and angle between the wind and current play a role. Western boundary currents, like the Kuroshio Current, have strong surface currents, resulting in a large response to the current feedback (CFB). Additionally, when synoptic low-pressure systems pass through

this area and wind speed and direction abruptly change, the CFB will also rapidly change.

Current coupling modifies the background states over the seasonal timescale. The immediate responses of the lower-level atmosphere to current coupling are expected to alter exchange coefficients and atmospheric stability, leading to further changes in conditions such as low-level wind and wind stress through complex interactions. As a result, after six months of integration, the angle between the wind and surface current is not the key factor for the differences in the wind stress and turbulent heat flux caused by current coupling. This is because current coupling modifies the background states of the atmosphere and ocean, such as the wind speed and SST. In particular, the differences in the air-sea fluxes become less sensitive to the angle in the area where the current speed exceeds 1 m/s. This area generally corresponds to the Kuroshio Extension, whose position diverges in the three simulations where current coupling was considered in different ways. This suggests that the accumulated immediate impacts of the current coupling were sufficiently large to change the background atmospheric and oceanic states in the seasonal timescale.

Although the impact of current coupling on the momentum flux has been explored in previous studies, the impact on the turbulent heat flux remains unexplored. Overall, current coupling reduces the current speed by either dragging the surface current when the wind is against the current or reducing the momentum input into the ocean when the wind and surface current move in the same direction. Current coupling similarly modulates the turbulent heat flux depending on the angle between the wind and current, but its impact on SST is limited. This can be attributed to the negative feedback caused by the anomalous SST. For example, if current coupling results in an increase in latent heat release at the sea surface and a cooling of the upper ocean, the anomalously cold SST leads to lower longwave upward radiation and lower turbulent heat flux, which alleviates the anomalously cold SST.

The position of the Kuroshio Extension diverges when either the momentum or turbulent heat flux is estimated without considering the surface current. The change through the former process is expected as the surface current accelerates when the current coupling is ignored in the wind stress calculation. However, the divergence of the path of the Kuroshio Extension through changes in the turbulent heat flux is

unexpected, considering that the net changes in the turbulent heat flux are considerably small and that the turbulent heat flux does not have a direct connection to the momentum budget of the upper ocean. We inferred that the small deviation of the turbulent heat flux can trigger complex atmosphere-ocean interactions and even alter the path of the Kuroshio Extension. We presumed that the upper ocean kinetic and potential energy were also modified by current coupling through the turbulent heat flux, which will be explored in a future study.

We demonstrated that on a seasonal timescale, current coupling can induce changes in the background states of the atmosphere and ocean and the fluxes between them through complex air-sea interactions. In particular, despite the insignificant changes in the net turbulent heat flux and SST, current coupling has a sizable impact, resulting in various shifts, including changes in the position of the Kuroshio Extension. Hence, enabling the feedback between the atmosphere and ocean is essential to capture the impact of the surface current, and the fully coupled ocean-atmosphere model is necessary to realize this objective.

CRediT authorship contribution statement

Ajin Cho: Writing – original draft, Visualization, Investigation, Formal analysis. **Hajoon Song:** Writing – review & editing, Supervision, Resources, Project administration, Methodology, Funding acquisition, Conceptualization. **Hyodae Seo:** Writing – review & editing, Methodology, Conceptualization. **Rui Sun:** Writing – review & editing, Software. **Matthew R. Mazloff:** Writing – review & editing, Software. **Aneesh C. Subramanian:** Writing – review & editing, Software. **Bruce D. Cornuelle:** Writing – review & editing, Software. **Arthur J. Miller:** Writing – review & editing, Software.

Funding sources

This work was supported by the National Research Foundation of Korea (NRF) grant funded by the Korea government (MSIT) (NRF-2022R1A2C1009792), and the Korea Meteorological Administration Research and Development Program (RS-2024-00404973). H. Seo acknowledges support from National Science Foundation, USA (OCE-2148120) and NOAA, USA (NA22OAR4310598). A.J. Miller was partly supported by the U.S. National Science Foundation (OCE2022868).

Declaration of competing interest

The authors declare the following financial interests/personal relationships which may be considered as potential competing interests: Hajoon Song reports financial support was provided by National Research Foundation of Korea. If there are other authors, they declare that they have no known competing financial interests or personal relationships that could have appeared to influence the work reported in this paper.

Appendix A. Supplementary data

Supplementary material related to this article can be found online at <https://doi.org/10.1016/j.ocemod.2024.102496>.

Data availability

The Scripps-KAUST Regional Integrated Prediction System (SKRIPS) v1.2 (Sun et al., 2019) is available at https://github.com/iurnus/scripps_kaust_model/releases/tag/v1.2. The configuration for this study can be obtained from <https://doi.org/10.5281/zenodo.11480617>.

References

- Chelton, D.B., Schlax, M.G., Freilich, M.H., Milliff, R.F., 2004. Satellite measurements reveal persistent small-scale features in ocean winds. *Science* 303 (5660), 978–983. <http://dx.doi.org/10.1126/science.1091901>.
- Cronin, M.F., Gentemann, C.L., Edson, J., Ueki, I., Bourassa, M., Brown, S., Clayton, C.A., Fairall, C.W., Farrar, J.T., Gille, S.T., Gulev, S., Josey, S.A., Kato, S., Katsumata, M., Kent, E., Krug, M., Minnett, P.J., Parfitt, R., Pinker, R.T., Stackhouse, P.W., Swart, S., Tomita, H., Vandemark, D., Weller, A.R., Yoneyama, K., Yu, L., Zhang, D., 2019. Air-sea fluxes with a focus on heat and momentum. *Front. Mar. Sci.* 6.
- Fairall, C.W., Bradley, E.F., Hare, J.E., Grachev, A.A., Edson, J.B., 2003. Bulk parameterization of air-sea fluxes: Updates and verification for the COARE algorithm. *J. Clim.* 16 (4), 571–591. [http://dx.doi.org/10.1175/1520-0442\(2003\)016<0571:BPOASF>2.0.CO;2](http://dx.doi.org/10.1175/1520-0442(2003)016<0571:BPOASF>2.0.CO;2).
- Foussard, A., Lapeyre, G., Plougmonen, R., 2019. Storm track response to oceanic eddies in idealized atmospheric simulations. *J. Clim.* 32 (2), 445–463. <http://dx.doi.org/10.1175/JCLI-D-18-0415.1>.
- Frenger, I., Gruber, N., Knutti, R., Münnich, M., 2013. Imprint of Southern Ocean eddies on winds, clouds and rainfall. *Nat. Geosci.* 6 (8), 608–612. <http://dx.doi.org/10.1038/ngeo1863>.
- Hersbach, H., Bell, B., Berrisford, P., Hirahara, S., Horányi, A., Muñoz-Sabater, J., Nicolas, J., Peubey, C., Radu, R., Schepers, D., Simmons, A., Soci, C., Abdalla, S., Abellán, X., Balsamo, G., Bechtold, P., Biavati, G., Bidlot, J., Bonavita, M., De Chiara, G., Dahlgren, P., Dee, D., Diamantakis, M., Dragani, R., Flemming, J., Forbes, R., Fuentes, M., Geer, A., Haimberger, L., Healy, S., Hogan, R.J., Hólm, E., Janisková, M., Keeley, S., Laloyaux, P., Lopez, P., Lupu, C., Radnoti, G., de Rosnay, P., Rozum, I., Vamborg, F., Villaume, S., Thépaut, J.-N., 2020. The ERA5 global reanalysis. *Q. J. R. Meteorol. Soc.* 146 (730), 1999–2049. <http://dx.doi.org/10.1002/qj.3803>.
- Hill, C., DeLuca, C., Balaji, Suarez, M., Da Silva, A., 2004. The architecture of the earth system modeling framework. *Comput. Sci. Eng.* 6 (1), 18–28. <http://dx.doi.org/10.1109/MCISE.2004.1255817>.
- Hong, S.-Y., Lim, J.-O.J., 2006. The WRF single-moment 6-class microphysics scheme (WSM6). *Asia-Pac. J. Atmos. Sci.* 42 (2), 129–151.
- Iacono, M.J., Delamere, J.S., Mlawer, E.J., Shepherd, M.W., Clough, S.A., Collins, W.D., 2008. Radiative forcing by long-lived greenhouse gases: Calculations with the AER radiative transfer models. *J. Geophys. Res.: Atmos.* 113 (D13), <http://dx.doi.org/10.1029/2008JD009944>.
- Jullien, S., Masson, S., Oerder, V., Samson, G., Colas, F., Renault, L., 2020. Impact of ocean-atmosphere current feedback on ocean mesoscale activity: Regional variations and sensitivity to model resolution. *J. Clim.* 33 (7), 2585–2602. <http://dx.doi.org/10.1175/JCLI-D-19-0484.1>.
- Kilpatrick, T., Schneider, N., Qiu, B., 2014. Boundary layer convergence induced by strong winds across a midlatitude SST front. *J. Clim.* 27 (4), 1698–1718. <http://dx.doi.org/10.1175/JCLI-D-13-00101.1>.
- Ma, X., Chang, P., Saravanan, R., Montuoro, R., Hsieh, J.-S., Wu, D., Lin, X., Wu, L., Jing, Z., 2015. Distant influence of kuroshio eddies on north Pacific weather patterns? *Sci. Rep.* 5 (1), 17785. <http://dx.doi.org/10.1038/srep17785>.
- Ma, X., Jing, Z., Chang, P., Liu, X., Montuoro, R., Small, R.J., Bryan, F.O., Greatbatch, R.J., Brandt, P., Wu, D., Lin, X., Wu, L., 2016. Western boundary currents regulated by interaction between ocean eddies and the atmosphere. *Nature* 535 (7613), 533–537. <http://dx.doi.org/10.1038/nature18640>.
- Marshall, J., Adcroft, A., Hill, C., Perelman, L., Heisey, C., 1997. A finite-volume, incompressible Navier Stokes model for studies of the ocean on parallel computers. *J. Geophys. Res.: Oceans* 102 (C3), 5753–5766. <http://dx.doi.org/10.1029/96JC02775>.
- Miobane, S., Kuwano-Yoshida, A., Komori, N., Xie, S.-P., Small, R.J., 2008. Influence of the gulf stream on the troposphere. *Nature* 452 (7184), 206–209. <http://dx.doi.org/10.1038/nature06690>.
- Nakanishi, M., Niino, H., 2004. An improved Mellor-Yamada level-3 model with condensation physics: Its design and verification. *Bound.-Layer Meteorol.* 112 (1), 1–31. <http://dx.doi.org/10.1023/B:BOUN.0000020164.04146.98>.
- Nakanishi, M., Niino, H., 2009. Development of an improved turbulence closure model for the atmospheric boundary layer. *J. Meteorol. Soc. Jpn. Ser. II* 87 (5), 895–912. <http://dx.doi.org/10.2151/jmsj.87.895>.
- O'Reilly, C.H., Czaja, A., 2015. The response of the Pacific storm track and atmospheric circulation to Kuroshio Extension variability. *Q. J. R. Meteorol. Soc.* 141 (686), 52–66. <http://dx.doi.org/10.1002/qj.2334>.
- Parfitt, R., Czaja, A., Minobe, S., Kuwano-Yoshida, A., 2016. The atmospheric frontal response to SST perturbations in the gulf stream region. *Geophys. Res. Lett.* 43 (5), 2299–2306. <http://dx.doi.org/10.1002/2016GL067723>.
- Parfitt, R., Seo, H., 2018. A new framework for near-surface wind convergence over the Kuroshio Extension and gulf stream in wintertime: The role of atmospheric fronts. *Geophys. Res. Lett.* 45 (18), 9909–9918. <http://dx.doi.org/10.1029/2018GL080135>.
- Pelletier, C., Lemarié, F., Blayo, E., Bouin, M.-N., Redelsperger, J.-L., 2021. Two-sided turbulent surface-layer parameterizations for computing air-sea fluxes. *Q. J. R. Meteorol. Soc.* 147 (736), 1726–1751. <http://dx.doi.org/10.1002/qj.3991>.

- Putrasahan, D.A., Miller, A.J., Seo, H., 2013. Isolating mesoscale coupled ocean-atmosphere interactions in the Kuroshio Extension region. *Dyn. Atmos. Oceans* 63, 60–78. <http://dx.doi.org/10.1016/j.dynatmoce.2013.04.001>.
- Renault, L., Masson, S., Oerder, V., Colas, F., McWilliams, J.C., 2023. Modulation of the oceanic mesoscale activity by the mesoscale thermal feedback to the atmosphere. *J. Phys. Oceanogr.* 53 (7), 1651–1667. <http://dx.doi.org/10.1175/JPO-D-22-0256.1>.
- Renault, L., Masson, S., Oerder, V., Jullien, S., Colas, F., 2019. Disentangling the mesoscale ocean-atmosphere interactions. *J. Geophys. Res.: Oceans* 124 (3), 2164–2178. <http://dx.doi.org/10.1029/2018JC014628>.
- Renault, L., McWilliams, J.C., Masson, S., 2017. Satellite observations of imprint of oceanic current on wind stress by air-sea coupling. *Sci. Rep.* 7 (1), 17747. <http://dx.doi.org/10.1038/s41598-017-17939-1>.
- Renault, L., Molemaker, M.J., McWilliams, J.C., Shchepetkin, A.F., Lemarié, F., Chelton, D., Illig, S., Hall, A., 2016. Modulation of wind work by oceanic current interaction with the atmosphere. *J. Phys. Oceanogr.* 46 (6), 1685–1704. <http://dx.doi.org/10.1175/JPO-D-15-0232.1>.
- Seo, H., Miller, A.J., Norris, J.R., 2016. Eddy-wind interaction in the California current system: Dynamics and impacts. *J. Phys. Oceanogr.* 46 (2), 439–459. <http://dx.doi.org/10.1175/JPO-D-15-0086.1>.
- Seo, H., Murtugudde, R., Jochum, M., Miller, A.J., 2008. Modeling of mesoscale coupled ocean-atmosphere interaction and its feedback to ocean in the western arabian sea. *Ocean Model.* 25 (3–4), 120–131. <http://dx.doi.org/10.1016/j.ocemod.2008.07.003>.
- Seo, H., O'Neill, L.W., Bourassa, M.A., Czaja, A., Drushka, K., Edson, J.B., Fox-Kemper, B., Frenger, I., Gille, S.T., Kirtman, B.P., Minobe, S., Pendergrass, A.G., Renault, L., Roberts, M.J., Schneider, N., Small, R.J., Stoffelen, A., Wang, Q., 2023. Ocean mesoscale and frontal-scale ocean-atmosphere interactions and influence on large-scale climate: A review. *J. Clim.* 36 (7), 1981–2013. <http://dx.doi.org/10.1175/JCLI-D-21-0982.1>.
- Seo, H., Subramanian, A.C., Song, H., Chowdary, J.S., 2019. Coupled effects of ocean current on wind stress in the bay of bengal: Eddy energetics and upper ocean stratification. *Deep Sea Res. II: Top. Stud. Oceanogr.* 168, 104617. <http://dx.doi.org/10.1016/j.dsr2.2019.07.005>.
- Shan, X., Jing, Z., Sun, B., Wu, L., 2020. Impacts of ocean current-atmosphere interactions on mesoscale eddy energetics in the Kuroshio extension region. *Geosci. Lett.* 7 (1), 3. <http://dx.doi.org/10.1186/s40562-020-00152-w>.
- Skamarock, C., Klemp, B., Dudhia, J., Gill, O., Liu, Z., Berner, J., Wang, W., Powers, G., Duda, G., Barker, D., Huang, X.-y., 2019. A description of the advanced research WRF model version 4.1. NCAR Tech. Note <http://dx.doi.org/10.5065/1dfh-6p97>.
- Small, R., deSzoeke, S., Xie, S., O'Neill, L., Seo, H., Song, Q., Cornillon, P., Spall, M., Minobe, S., 2008. Air-sea interaction over ocean fronts and eddies. *Dyn. Atmos. Oceans* 45 (3–4), 274–319. <http://dx.doi.org/10.1016/j.dynatmoce.2008.01.001>.
- Song, H., Marshall, J., McGillicuddy, D.J., Seo, H., 2020. Impact of current-wind interaction on vertical processes in the Southern Ocean. *J. Geophys. Res.: Oceans* 125 (4), <http://dx.doi.org/10.1029/2020JC016046>.
- Sun, R., Subramanian, A.C., Miller, A.J., Mazloff, M.R., Hoteit, I., Cornuelle, B.D., 2019. SKRIPS v1.0: a regional coupled ocean-atmosphere modeling framework (MITgcm-WRF) using ESMF/NUOPC, description and preliminary results for the Red Sea. *Geosci. Model Dev.* 12 (10), 4221–4244. <http://dx.doi.org/10.5194/gmd-12-4221-2019>.
- Tomita, H., Hihara, T., Kako, S., Kubota, M., Kutsuwada, K., 2019. An introduction to J-OFURO3, a third-generation Japanese ocean flux data set using remote-sensing observations. *J. Oceanogr.* 75 (2), 171–194. <http://dx.doi.org/10.1007/s10872-018-0493-x>.
- Zuo, H., Balmaseda, M.A., Tietsche, S., Mogensen, K., Mayer, M., 2019. The ECMWF operational ensemble reanalysis-analysis system for ocean and sea ice: a description of the system and assessment. *Ocean Sci.* 15 (3), 779–808. <http://dx.doi.org/10.5194/os-15-779-2019>.